Bergische Universität Wuppertal

Fakultät für Mathematik und Naturwissenschaften

Institute of Mathematical Modelling, Analysis and Computational Mathematics (IMACM)

Preprint BUW-IMACM 20/47

H. Fatoorehchi and M. Ehrhardt

Numerical and semi-numerical solutions of a modified Thévenin model with application to the dynamic analysis of electrochemical batteries

October 22, 2020

http://www.imacm.uni-wuppertal.de

Numerical and semi-numerical solutions of a modified Thévenin model with application to the dynamic analysis of electrochemical batteries

Hooman Fatoorehchi [a*], Matthias Ehrhardt [b*]

[a] School of Chemical Engineering, College of Engineering, University of Tehran, P.O. Box 11365-4563, Tehran, Iran

[b] Chair of Applied Mathematics and Numerical Analysis, University of Wuppertal, Gaußstrasse 20, D-42119, Wuppertal, Germany

[*] Correspondence: hfatoorehchi@ut.ac.ir, ehrhardt@uni-wuppertal.de

Abstract- A new Thévenin-type model for the dynamics of an electrochemical battery is developed by adding a nonlinear capacitor element in the circuit. Furthermore, a powerful variant of the improved differential transform method and the nonstandard finite difference schemes are proposed to properly treat the mathematical model. Two separate case studies including a constant and a variable current consumer, which represents an inductive electric motor, are carried out. The efficacies of the multistage improved differential transform method, the nonstandard finite difference schemes, and the classical Euler method are compared using a set of appropriate CPU-time and error analyses.

Keywords: Thévenin model, battery dynamics, improved differential transform method, nonstandard finite difference scheme, nonlinear capacitance.

1. Introduction

The dynamic characteristics of electrochemical batteries is a crucial factor in the design and operation of battery-powered systems. In this regard, mathematical models can be helpful at predicting the battery performance and lifetime as well as enabling an intelligent power management. These features are essential, particularly for battery-driven vehicles [1,2].

One of the leading models for the discharge dynamics of different types of batteries, viz., lead-acid, lithium-ion (Li-ion), lithium-polymer (Li-polymer), nickel metal hybrid (NiMH), and fuel cells, is the Thévenin battery model [3]. Conceptually, the Thévenin model is comprised of an ideal voltage source, and internal resistance, an over-charge resistance, and a capacitance, where the two latter elements are connected in parallel. The parameters in the Thévenin model are considered constant for simplicity although they vary as the rate of electrochemical reactions inside the battery changes with the state of charge (SOC), ambient temperature, battery storage capacity, external load, age of the battery, etc. [4]. The aforementioned shortcoming of the Thévenin battery model can practically be overcome by periodically updating the model parameters using the online experimental data at a suitable frequency. Consequently, the accurate evaluation of the model parameters is an emerging concern for reliable control of battery-powered systems. Several approaches such as parameter identification algorithms [5], the extended Kalman filter algorithm [6-8], the neural network algorithm [9], and fuzzy logic-based strategies [8-11] have been proposed in the literature in this regard. Elaborate discussions on the performance and efficacy of available dynamical models for batteries are presented in [12,13].

In this paper, we have generalized the classical Thévenin model by incorporating a nonlinear capacitor in its equivalent circuit. Subsequently, we have analyzed the performance of our proposed model by several numerical and semi-analytical mathematical methods including the classical Euler integrator, the nonstandard finite difference (NSFD) schemes, and the multistage improved differential transform method for two different scenarios: 1) the case of constant load, and 2) the case of an inductive load. The relevant error analyses and computational evaluations are given for a real-world case study in the sequel.

2. Mathematical preliminaries

2.1. The fundamentals of the multistage improved differential transform method

The differential transform method (DTM) was first presented independently by Zhou and Pukhov in 1986 [14,15] in a systematic framework. The method is capable of presenting the solution of a single functional equation or a system of functional equations in terms of infinite series, provided that the solution is analytic. The procedure of the DTM is as follows: First, the functional equation is mapped to a new domain by the differential transform. Next, the transformed equation is solved by establishing a recursive relation using simple algebraic operations. Finally, the inverse differential transform is applied to obtain the solution in the original domain.

The one-dimensional differential transform of a given function $u(t)$ is defined by

$$DT\{u(t)\} = U(k) = \frac{1}{k!}\left[\frac{d^k u(t)}{dt^k}\right]_{t=t_i}, \tag{1}$$

and the corresponding inverse differential transform is defined as

$$u(t) = DT^{-1}\{U(k)\} = \sum_{k=0}^{+\infty} U(k)(t-t_i)^k. \tag{2}$$

In Eq. (1), it is assumed that the function $u(t)$ is analytic in a domain D and t_i represents any point in the domain D. Also, k is a non-negative integer.

As it is perceivable, the DTM does not require any discretization, linearization, or perturbation. In 2013, Fatoorehchi and Abolghasemi [16] extended the DTM for solving nonlinear equations and proposed the improved differential transform method (IDTM). This improvement was achieved by incorporating the Adomian polynomials in the classical DTM.

Let us consider a general nonlinear differential equation in the following operator form,

$$\frac{du^n}{dt^n} = N(u) + r(u) + g, \tag{3}$$

where r is the linear differential operator of an order less than n, N is a nonlinear operator from a Hilbert space H to itself, and g denotes a specified function of H. We are looking for $u \in H$ such that it satisfies Eq. (3).

If we take the differential transform of both sides of Eq. (3), we obtain

$$\frac{(k+n)!}{k!}U(k+n) = DT\{N(u)\} + DT\{r(u)\} + DT\{g\}. \tag{4}$$

It can be proved [12], that

$$DT\{N(u)\} = A_k(U(0), U(1), \ldots, U(k)), \tag{5}$$

where the A_i are called the Adomian polynomials [17] that decompose the nonlinear operator H such that $N(u)=\sum_{i=0}^{+\infty}A_i$, and they can be calculated by the following formula:

$$A_i = A_i(u_0,u_1,\ldots,u_i) = \frac{1}{i!}\frac{d^i}{d\lambda^i}N\left(\sum_{k=0}^{+\infty}u_k\lambda^k\right)\Bigg|_{\lambda=0}, \tag{6}$$

where the u_i are components constituting the solution u, i.e., $u=\sum_{i=0}^{+\infty}u_i$.

Thus, it follows from Eq. (4) that

$$U(k+n)=\frac{k!}{(k+n)!}\Big[A_k\left(U(0),U(1),\ldots,U(k)\right)+R(k)+G(k)\Big],\quad k\geq 0, \tag{7}$$

where $R(k)=DT\{r(u)\}$ and $G(k)=DT\{g\}$.

The other components of $U(k)$ with $k=0, \ldots, n-1$ can be determined from the n initial conditions of Eq. (3).

Consequently, the solution is conveniently obtained by a simple inversion:

$$u(t)=DT^{-1}\{U(k)\}=\sum_{k=0}^{+\infty}U(k)(t-t_i)^k. \tag{8}$$

In practice, we have to truncate the infinite series (8) and accept an approximate solution like

$$u\approx\psi_{m,i}=\sum_{k=0}^{m-1}U(k)(t-t_i)^k. \tag{9}$$

It is straightforward to see that the partial sum (9) is convergent in the vicinity of t_i and it may diverge or be prone to large errors as t exceeds t_i. Particularly, in the case of differential equations with semi-infinite domains, which include almost all dynamic problems of physics and engineering, the solution (9) is not reliable. Hence, we now propose a multistage variation of the IDTM.

In this approach, we divide the domain of the independent variable into a number of intervals. Starting from the first interval, we solve Eq. (3) together with the original initial conditions using Eq. (9) with $t_i=t_0$. Next, we solve Eq. (3) for the subsequent interval using the final data points of the solution in the previous interval as the initial conditions and taking $t_i=t_1$. This step is repeated until the desired upper bound of the solution is reached. The time-marching concept of the IDTM is visualized in Fig. 1. For more backgrounds and applications of the DTM and the IDTM, the interested reader may consult the literature [18-22].

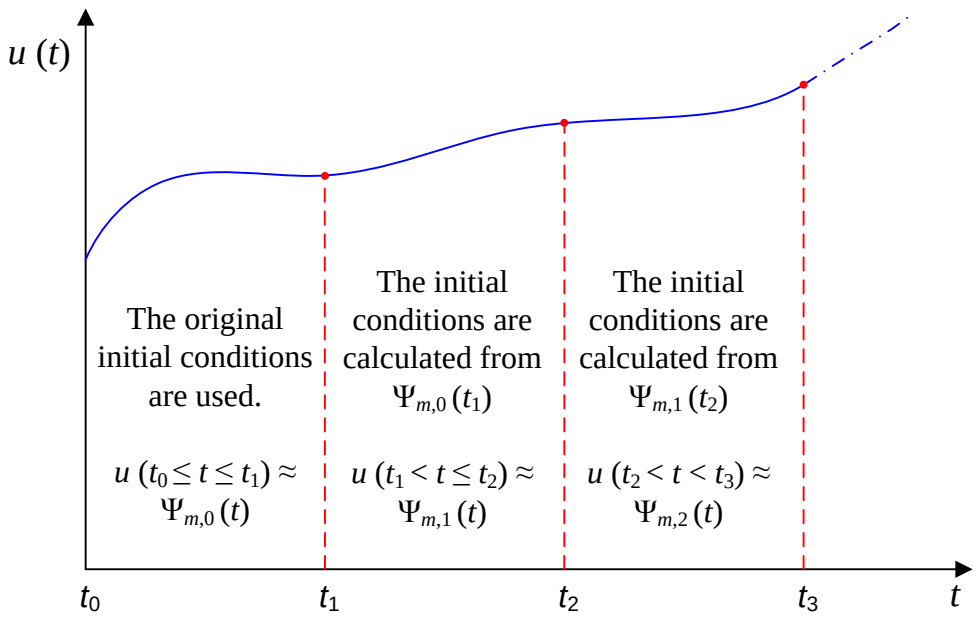

Fig. 1) Conceptual visualization of the multistage improved differential transform method.

2.2. The fundamentals of the nonstandard finite difference scheme

Let us consider a first-order differential equation of the following type,

$$\frac{du}{dt} = f(t,u), \quad u(t_0) = u_0, \tag{10}$$

where $u:[t_0,T)\to\mathbb{R}$ and $f:([t_0,T),\mathbb{R})\to([t_0,T),\mathbb{R})$.

First, we discretize the independent variable t by $t_k = t_0 + hk$, where h is a preferably small positive step size. Now, if we denote the discretized version of u at time t_k by u_k, then the discretized analog of Eq. (10) becomes

$$D_h u_k = F_k(t_k, f, u_k), \tag{11}$$

where $D_h u_k$ is the discretization of du/dt, and $F_k(t_k, f, u_k)$ denotes the approximation of $f(t_k, u_k)$.

The numerical scheme proposed as in Eq. (11) is of the nonstandard finite difference family if the following conditions are fulfilled [23,24]:

1- The discretization of the first-order derivative is performed by

$$D_h u_k = \frac{u_{k+1} - \psi u_k}{\phi}, \tag{12}$$

where the functions ψ and ϕ depend on the step size and satisfy the following conditions:

$$\psi = 1 + O(h), \quad \phi = h + O(h^2), \text{ for } h \to 0. \tag{13}$$

2- The nonlinear terms should be replaced by their nonlocal discrete counterparts.

In summary, the NSFD entails a more sophisticated discretization of the derivative operators, to mitigate the usual instabilities associated with the classical finite difference method. It mimics the qualitative behavior of the solution on a discrete level.

A set of rules and recommendations for the construction of a robust NSFD has been proposed by Mickens in [23,24]. Expository examples on the application of NSFD in mathematical models of various scientific and engineering disciplines can be found in the recent literature [25-28].

3. The proposed model and solution

3.1. The mathematical model for the constant load case

Let us consider our modified Thévenin model of a discharging battery as depicted in Fig 2.

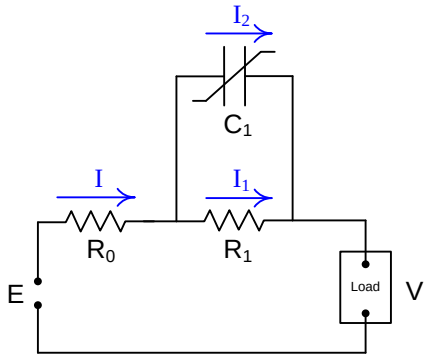

Fig. 2) The schematic view of the Thévenin model with a nonlinear capacitor; the constant electric current case.

The battery is connected to a consumer load of constant current. In practice, such a constant current is realized by the action of an electric current controller unit placed in series to the consumer.

We assume that the capacitor C_1 is nonlinear and its charge-voltage characteristics is given by,

$$Q_1 = k_1 \arctan\left(k_2 V_{C_1} + k_3\right) + k_4, \tag{14}$$

where k_1, k_2, k_3, and k_4 are empirical constants. Other dependencies can be considered [29].

It follows from Kirchhoff's current law (KCL) that at any time the total constant current is equal to the sum of currents passing through each branches of the R_1C_1 loop,

$$I = I_1 + I_2 . \tag{15}$$

Also, we can write from Kirchhoff's voltage law (KVL) in the RC loop that

$$R_1\left(I - I_2\right) = V_{C_1} . \tag{16}$$

Putting $I_2 = dQ/dt$ in Eq. (16), we obtain

$$R_1 I - R_1 \frac{dQ}{dt} = V_{C_1} . \tag{17}$$

Next, we take the derivative of Eq. (14) with respect to t,

$$\frac{dQ}{dt} = \frac{k_1 k_2}{k_2^2 V_{C_1}^2 + 2k_2 k_3 V_{C_1} + k_3^2 + 1} \frac{dV_{C_1}}{dt} . \tag{18}$$

From Eqs. (17) and (18), we conclude that

$$\frac{dV_{C_1}}{dt} = -\frac{k_2}{R_1 k_1} V_{C_1}^3 + \frac{R_1 I k_2 - 2k_3}{R_1 k_1} V_{C_1}^2 + \frac{2k_2 k_3 R_1 I - k_3^2 - 1}{R_1 k_1 k_2} V_{C_1} + \frac{k_3^2 I + I}{k_1 k_2} . \tag{19}$$

If we have the dynamics of the capacitor voltage, the delivering voltage of the battery can be easily computed as

$$V = E - R_0 I - V_{C_1}\,. \tag{20}$$

The Simulink® model of Eq. (19) is given in Fig (3).

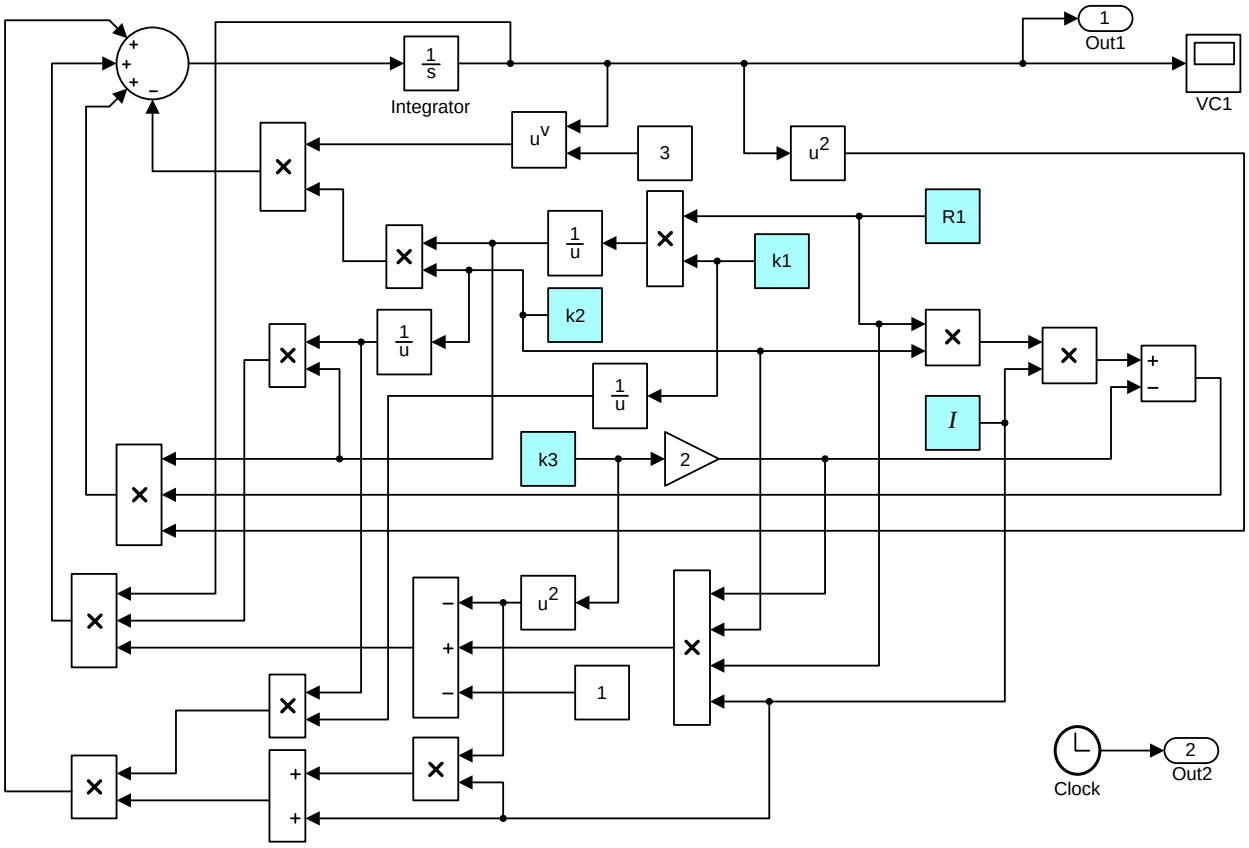

Fig. 3) The block diagram representation of the capacitor voltage in the modified Thévenin model [Eq. (19)].

3.1.1. Analysis by the multistage improved differential transform method

For better notion, let us take $u = V_{C_1}$ in Eq. (19) and take the differential transform of its both sides to obtain

$$(k+1)U(k+1) = aDT\left\{u^3\right\} + bDT\left\{u^2\right\} + cU(k) + d\,\delta(k)\,. \tag{21}$$

According to the basics of the multistage IDTM, it follows from Eq. (21) that

$$\begin{aligned}(k+1)U(k+1) &= aA_k\left(U(0),\ldots,U(k)\right) + bB_k\left(U(0),\ldots,U(k)\right)\\ &+cU(k) + d\,\delta(k),\end{aligned} \tag{22}$$

where A_i and B_i denote the Adomian polynomials decomposing nonlinear operators $N_1(u) = u^3$, and $N_2(u) = u^2$, respectively. In other words,

$$u^3 = \sum_{i=0}^{+\infty} A_i\left(u_0,\ldots,u_i\right), \tag{23}$$

$$u^2 = \sum_{i=0}^{+\infty} B_i\left(u_0,\ldots,u_i\right). \tag{24}$$

So, we can rearrange Eq. (22),

$$U(k+1)=\frac{aA_k\left(U(0),\ldots,U(k)\right)+bB_k\left(U(0),\ldots,U(k)\right)+cU(k)+d\delta(k)}{k+1},\quad k\geq 0, \tag{25}$$

and have the solution as,

$$u=V_{C_1}(t)=DT^{-1}\left\{U(k)\right\}=\sum_{k=0}^{+\infty}U(k)(t-t_i)^k. \tag{26}$$

We can set up the multistage variant of Eq. (26) as follows

$$\begin{cases} u(t_0\leq t\leq t_0+h)\approx\sum_{k=0}^{m-1}U(k)(t-t_0)^k, \\ U(0)=u_0 \\ U(k+1)=\dfrac{aA_k\left(U(0),\ldots,U(k)\right)+bB_k\left(U(0),\ldots,U(k)\right)+cU(k)+d\delta(k)}{k+1}, \quad 0\leq k\leq m-2 \end{cases}$$

$$\begin{cases} u(t_0+h<t\leq t_0+2h)\approx\sum_{k=0}^{m-1}U(k)(t-t_0-h)^k, \\ U(0)=u(h) \\ U(k+1)=\dfrac{aA_k\left(U(0),\ldots,U(k)\right)+bB_k\left(U(0),\ldots,U(k)\right)+cU(k)+d\delta(k)}{k+1}, \quad 0\leq k\leq m-2 \end{cases} \tag{27}$$

$$\begin{cases} u(t_0+2h<t\leq t_0+3h)\approx\sum_{k=0}^{m-1}U(k)(t-t_0-2h)^k, \\ U(0)=u(2h) \\ U(k+1)=\dfrac{aA_k\left(U(0),\ldots,U(k)\right)+bB_k\left(U(0),\ldots,U(k)\right)+cU(k)+d\delta(k)}{k+1}, \quad 0\leq k\leq m-2 \end{cases}$$

$\vdots$

where $h=\Delta t$ is a preferably small time step size and δ denotes the Kronecker delta function.

3.1.2. Analysis by the Nonstandard Finite Difference Scheme

For simplicity of notation, let us consider Eq. (19) of the form,

$$\frac{du}{dt}=a\,u^3+b\,u^2+c\,u+d\,, \tag{28}$$

where obviously,

$$
\begin{aligned}
a &= -\frac{k_2}{R_1 k_1}, \\
b &= \frac{R_1 I k_2 - 2k_3}{R_1 k_1}, \\
c &= \frac{2k_2 k_3 R_1 I - k_3^2 - 1}{R_1 k_1 k_2}, \\
d &= \frac{k_3^2 I + I}{k_1 k_2}.
\end{aligned} \tag{29}
$$

According to the NSFD, we can discretize Eq. (28) with respect to time as follows

$$\frac{u_{n+1} - u_n}{\phi} = a u_n^2 u_{n+1} + b u_n u_{n+1} + c u_{n+1} + d\,, \tag{30}$$

where ϕ denotes the positive denominator function,

$$\phi(h) = \exp(h) - 1, \tag{31}$$

and the temporal nodes are given by

$$t_n = n\Delta t = nh. \tag{32}$$

If we solve Eq. (30) for u_{n+1}, we will obtain the explicit numerical solution of Eq. (19) as

$$u_{n+1} = \frac{d + \dfrac{u_n}{\exp(h) - 1}}{\dfrac{1}{\exp(h) - 1} - a u_n^2 - b u_n - c} = \frac{u_n + \big(\exp(h) - 1\big) d}{1 - \big(\exp(h) - 1\big)\big(a u_n^2 + b u_n + c\big)}, \tag{33}$$

which is computationally efficient.

3.1.3. Case Study I

A case study was carried out to evaluate the performance of the aforementioned methods, namely the multistage IDTM and the NSFD method together with the classical Euler method. The model parameters for the case study are listed in Table 1. The temporal variation of the capacitor voltage is depicted in Figure 4. Qualitatively, it can be observed that the multistage IDTM has excelled at solving the nonlinear ODE-based dynamical model compared with the other studied methods.

Table 1) The model parameters used in case study I.

Parameter	Value (Unit)	Parameter	Value (Unit)
k_1	0.001551	I	10 (mA)
k_2	0.2818	R_1	500 (Ω)
k_3	−0.9754		
k_4	0.001177		

Note: The parameters of the nonlinear capacitor model are obtained from fitting the experimental data [29].

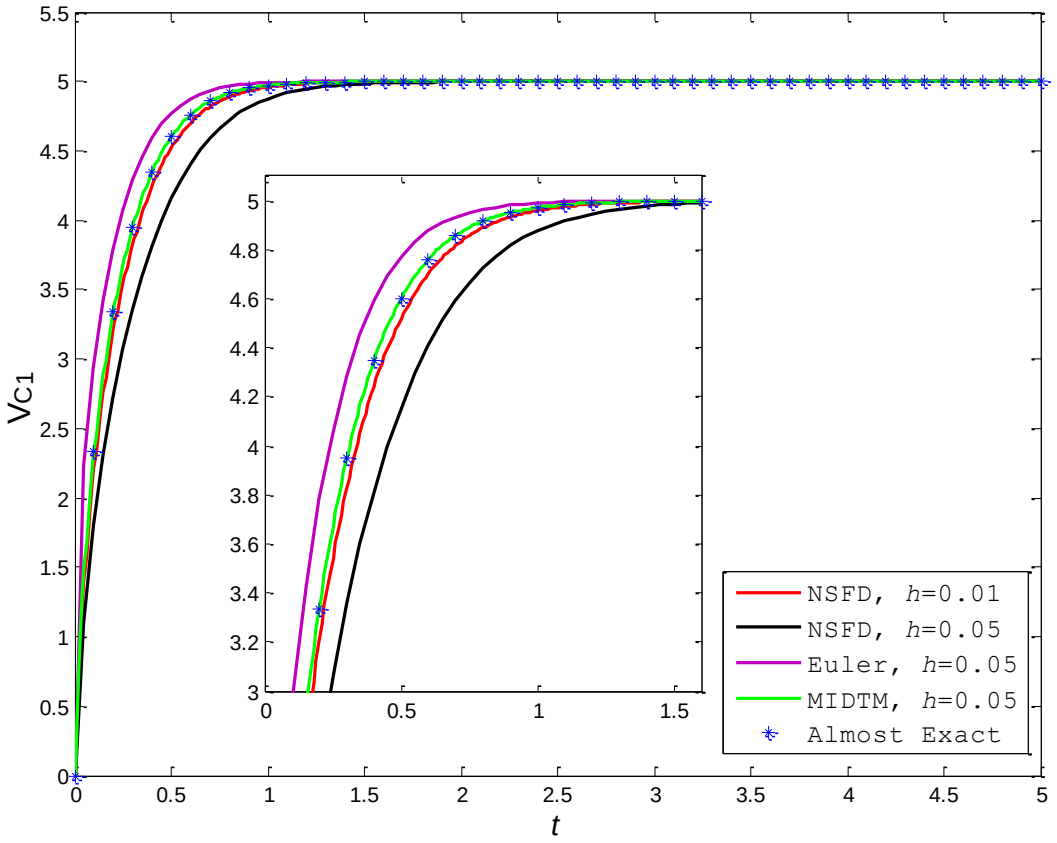

Figure 4) The solution of Eq. (19) by the NSFD method, the Euler method, and the multistage improved differential transform method.

3.1.4. Error Analysis

Upon close scrutiny, we find that Eq. (28) can be integrated to yield an implicit analytical relation between u and t.

$$\int \frac{du}{a\,u^3 + b\,u^2 + c\,u + d} = \int dt\,, \tag{34}$$

which leads to

$$\sum_{i=1}^{3} r_i \ln\left(9da^2r_i^2 + abr_i - abcr_i^2 + \left(3r_i a^2 - 2ab2r_i^2 + 6a^2cr_i^2\right)u\right) = t + C\,, \tag{35}$$

where C is the integration constant and r_i are the roots of the following cubic polynomial in x:

$$\left(-27a^2d^2 + 18abcd - 4ac^3 - 4b^3d + b^2c^2\right)x^3 + \left(3ac - b^2\right)x + a = 0\,. \tag{36}$$

Since, the capacitor is free of charge in the beginning; the initial condition $u(0) = 0$ is used to evaluate C as

$$C = \sum_{i=1}^{3} r_i \ln\left(9da^2r_i^2 + abr_i - abcr_i^2\right). \tag{37}$$

Substituting Eq. (37) in Eq. (35), we obtain

$$\sum_{i=1}^{3} r_i \left[\ln\left(\frac{9da^2 r_i^2 + abr_i - abcr_i^2 + \left(3r_i a^2 - 2ab2r_i^2 + 6a^2 cr_i^2\right)u}{9da^2 r_i^2 + abr_i - abcr_i^2} \right) \right] = t \,. \tag{38}$$

Consequently, we can define two types of error for our numerical results from Eq. (38). First, the sum of the absolute residuals (SAR) is defined by

$$E(N) = \sum_{n=0}^{N} \left| \sum_{i=1}^{3} r_i \left[\ln\left(\frac{9da^2 r_i^2 + abr_i - abcr_i^2 + \left(3r_i a^2 - 2ab2r_i^2 + 6a^2 cr_i^2\right)u_n}{9da^2 r_i^2 + abr_i - abcr_i^2} \right) \right] - t_n \right|, \tag{39}$$

where $t_n = nh$ as mentioned above.

Second, the average of the sum of the absolute residuals (ASAR) is defined by

$$\bar{E}(N) = \frac{1}{N+1} E(N) \,. \tag{40}$$

The results of the error analysis for solving the mathematical model at the constant load condition are tabulated; see Table 2.

Table 2) Error analysis results of Eq. (19) for the time interval [0 5].

Method	***h***	$E(N)$	$\bar{E}(N)$	**CPU-time***
NSFD	0.001	0.0757	0.0015	0.070549
Euler		0.0342	6.8400e-04	0.072267
MIDTM		1.8676e-13	3.7352e-15	1104.654
NSFD	0.01	0.7650	0.0153	0.002153
Euler		0.3506	0.0070	0.002261
MIDTM		3.5418e-13	7.0837e-15	45.5232
NSFD	0.05	3.9611	0.0792	0.000460
Euler		2.1123	0.0422	0.000464
MIDTM		0.0406	8.1200e-04	0.128960
NSFD	0.1	8.1289	0.1626	0.000254
Euler		5.9551	0.1191	0.000524
MIDTM		Diverges	Diverges	Diverges
NSFD	0.2	3.7482	0.0750	0.000139
Euler		Diverges	Diverges	0.000140
MIDTM		Diverges	Diverges	-
NSFD	0.5	1.3407	0.0268	0.000068
Euler		Diverges	Diverges	-
MIDTM		Diverges	Diverges	-

* CPU-times are measured in seconds on a personal computer with a 2.66 GHz Intel® Core 2 Duo processor and 2.00 GB of RAM.

It can be deduced from Table 2 that one remarkable advantage of the NSFD method is that its convergence is independent of the step size, also referred to as the mesh size, while being computationally fast. By choosing a sufficiently small step size, the NFSD can provide accurate results with an economic CPU-time. The multistage IDTM appears to be extremely accurate, i.e. about several orders of magnitude more accurate than the NSFD method. The main drawback, however, is its time-consuming nature, which originates from the need for preserving the solution coefficients up to a large number of digits and the long mathematical expressions of the incorporated Adomian polynomials. The classical Euler method is expectedly accurate at small step sizes, but diverges as they increase.

3.2. The mathematical model for the inductive load case

As shown in Fig. 5, this case models an inductive load, which can be any electrical motor as the consumer.

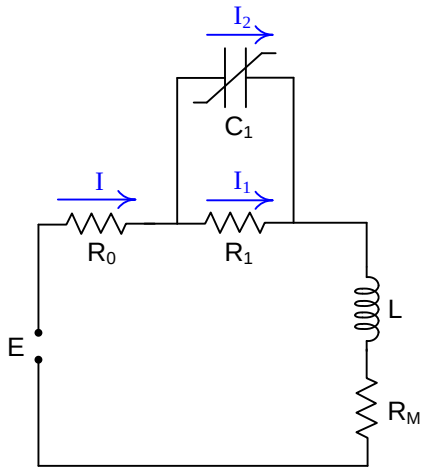

Fig. 5) The schematic view of the Thévenin model with a nonlinear capacitor; the inductive load case (resembles an electromotor).

The mathematical model of this case consists of a system of nonlinear ODEs as follows:

$$\begin{cases} \dfrac{dI}{dt} = \dfrac{E}{L} - \dfrac{\left(R_0 + R_M\right)}{L} I - \dfrac{1}{L} V_{C_1}, \\ \dfrac{dV_{C_1}}{dt} = -\dfrac{k_2}{R_1 k_1} V_{C_1}^3 + \dfrac{R_1 I k_2 - 2k_3}{R_1 k_1} V_{C_1}^2 + \dfrac{2k_2 k_3 R_1 I - k_3^2 - 1}{R_1 k_1 k_2} V_{C_1} + \dfrac{k_3^2 I + I}{k_1 k_2}. \end{cases} \tag{41}$$

Note that for this case, the electric current is not constant and changes with time. For the simplicity of notation, let us use the following variable changes

$$\begin{aligned} &\alpha = \frac{E}{L}, \quad \beta = -\frac{\left(R_0 + R_M\right)}{L}, \quad \gamma = -\frac{1}{L}, \\ &a = -\frac{k_2}{R_1 k_1}, b = \frac{k_2}{k_1}, \quad c = -2\frac{k_3}{R_1 k_1}, \quad d = 2\frac{k_3}{k_1}, \quad e = -\frac{k_3^2 + 1}{R_1 k_1 k_2}, \quad f = \frac{k_3^2 + 1}{k_1 k_2}, \end{aligned} \tag{42}$$

to yield

$$\begin{cases} \dfrac{dI}{dt} = \alpha + \beta I + \gamma u, \\ \dfrac{du}{dt} = a u^3 + b u^2 I + c u^2 + d u I + e u + f I. \end{cases} \tag{43}$$

The Simulink® model of Eq. (41) is depicted in Fig (6).

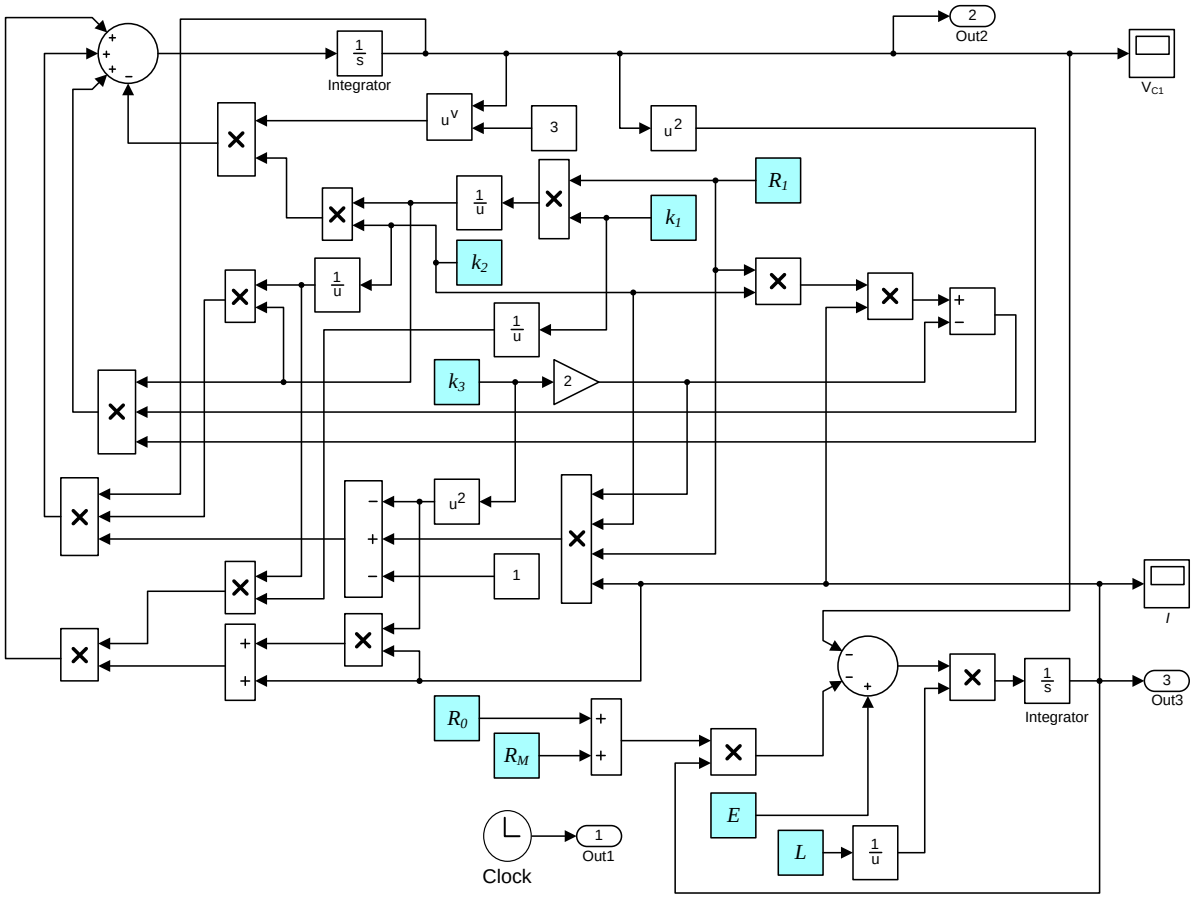

Fig. 6) The block diagram of the system of the ODEs for the inductive load case [Eq. (41)].

3.2.1. Analysis by the multistage improved differential transform method

In knowledge of section 2.1., we can take the differential transform of (43) and obtain

$$\begin{cases} (k+1)\bar{I}(k+1) = \alpha\delta(k) + \beta\bar{I}(k) + \gamma U(k), \\ (k+1)U(k+1) = a\,A_k\left(U(0),\ldots,U(k)\right) + b\sum_{r=0}^{k}\left\{B_r\left(U(0),\ldots,U(r)\right)\bar{I}(k-r)\right\} \\ +c\,B_k\left(U(0),\ldots,U(k)\right) + d\sum_{r=0}^{k}\left\{U(r)\bar{I}(k-r)\right\} + eU(k) + f\bar{I}(k). \end{cases} \tag{44}$$

or equivalently,

$$\begin{cases} \bar{I}(k+1) = \dfrac{\alpha\delta(k) + \beta\bar{I}(k) + \gamma U(k)}{k+1}, \\ U(k+1) = \dfrac{1}{k+1}\Big[a A_k\big(U(0),\ldots,U(k)\big) + b\sum\limits_{r=0}^{k}\big\{B_r\big(U(0),\ldots,U(r)\big)\bar{I}(k-r)\big\} \\ + c B_k\big(U(0),\ldots,U(k)\big) + d\sum\limits_{r=0}^{k}\big\{U(r)\bar{I}(k-r)\big\} + eU(k) + f\bar{I}(k)\Big]. \end{cases} \tag{45}$$

Note that the A_k and B_k represent the Adomian polynomials and are the same as defined previously by Eqs. (23) and (24).

In the multistage version, Eq. (45) becomes

$$\begin{cases} I\big(t_0 \le t \le t_0 + h\big) \approx \sum\limits_{k=0}^{m-1}\bar{I}(k)\big(t - t_0\big)^k, \\ u\big(t_0 \le t \le t_0 + h\big) \approx \sum\limits_{k=0}^{m-1}U(k)\big(t - t_0\big)^k, \\ \bar{I}(0) = I(t_0), \\ U(0) = u(t_0), \\ \bar{I}(k+1) = \dfrac{\alpha\delta(k) + \beta\bar{I}(k) + \gamma U(k)}{k+1}, \quad 0 \le k \le m-2, \\ U(k+1) = \dfrac{1}{k+1}\Big[a A_k\big(U(0),\ldots,U(k)\big) + b\sum\limits_{r=0}^{k}\big\{B_r\big(U(0),\ldots,U(r)\big)\bar{I}(k-r)\big\}, \\ + c B_k\big(U(0),\ldots,U(k)\big) + d\sum\limits_{r=0}^{k}\big\{U(r)\bar{I}(k-r)\big\} + eU(k) + f\bar{I}(k)\Big], \quad 0 \le k \le m-2 \end{cases}$$

$$\begin{cases} I\big(t_0 + h \le t \le t_0 + 2h\big) \approx \sum\limits_{k=0}^{m-1}\bar{I}(k)\big(t - t_0 - h\big)^k, \\ u\big(t_0 + h \le t \le t_0 + 2h\big) \approx \sum\limits_{k=0}^{m-1}U(k)\big(t - t_0 - h\big)^k, \\ \bar{I}(0) = I(h), \\ U(0) = u(h), \\ \bar{I}(k+1) = \dfrac{\alpha\delta(k) + \beta\bar{I}(k) + \gamma U(k)}{k+1}, \quad 0 \le k \le m-2, \\ U(k+1) = \dfrac{1}{k+1}\Big[a A_k\big(U(0),\ldots,U(k)\big) + b\sum\limits_{r=0}^{k}\big\{B_r\big(U(0),\ldots,U(r)\big)\bar{I}(k-r)\big\}, \\ + c B_k\big(U(0),\ldots,U(k)\big) + d\sum\limits_{r=0}^{k}\big\{U(r)\bar{I}(k-r)\big\} + eU(k) + f\bar{I}(k)\Big], \quad 0 \le k \le m-2 \end{cases} \tag{46}$$

$$
\begin{cases}
I\left(t_0+2h\le t\le t_0+3h\right)\approx\sum_{k=0}^{m-1}\bar{I}\left(k\right)\left(t-t_0-2h\right)^k,\\
u\left(t_0+2h\le t\le t_0+3h\right)\approx\sum_{k=0}^{m-1}U\left(k\right)\left(t-t_0-2h\right)^k,\\
\bar{I}\left(0\right)=I\left(2h\right),\\
U\left(0\right)=u\left(2h\right),\\
\bar{I}\left(k+1\right)=\dfrac{\alpha\delta\left(k\right)+\beta\bar{I}\left(k\right)+\gamma U\left(k\right)}{k+1},\quad 0\le k\le m-2,\\
U\left(k+1\right)=\dfrac{1}{k+1}\Big[a\,A_k\left(U\left(0\right),\ldots,U\left(k\right)\right)+b\sum_{r=0}^{k}\left\{B_r\left(U\left(0\right),\ldots,U\left(r\right)\right)\bar{I}\left(k-r\right)\right\},\\
+c\,B_k\left(U\left(0\right),\ldots,U\left(k\right)\right)+d\sum_{r=0}^{k}\left\{U\left(r\right)\bar{I}\left(k-r\right)\right\}+eU\left(k\right)+f\,\bar{I}\left(k\right)\Big],\quad 0\le k\le m-2
\end{cases}
$$

$$\vdots$$

3.2.2. Analysis by the Nonstandard Finite Difference Scheme

Based on the methodology of the NSFD, we can discretize the system of nonlinear ODEs (43) as

$$\frac{I_{n+1}-I_n}{\phi\left(h\right)}=\alpha+\beta I_{n+1}+\gamma u_n, \tag{47}$$

$$\frac{u_{n+1}-u_n}{\phi\left(h\right)}=a\,u_n^2u_{n+1}+bu_nu_{n+1}I_{n+1}+cu_nu_{n+1}+du_{n+1}I_{n+1}+eu_{n+1}+f\,I_{n+1}. \tag{48}$$

Next, we solve Eq. (47) for I_{n+1}

$$I_{n+1}=\frac{I_n+\alpha\phi+\gamma\phi u_n}{1-\beta\phi}\,. \tag{49}$$

Afterwards, we solve Eq. (48) for u_{n+1} as

$$u_{n+1}=\frac{u_n+\phi f\,I_{n+1}}{1-\phi\left(a\,u_n^2+bu_nI_{n+1}+c\,u_n+d\,I_{n+1}+e\right)}. \tag{50}$$

For simplicity, we choose again $\phi\left(h\right)=\exp\left(h\right)-1$, and obtain the solution in a recursive manner by using Eqs. (49) and (50) orderly. The scheme (49)-(50) is explicit and straightforward.

3.2.3. Case Study II

The situation when the battery is connected to an inductive element can be of specific interest as most of the commercial electric motors have non-negligible inductance. To appraise the performance of the aforementioned numerical and semi-numerical methods, a second case study was conducted using the model parameters as listed in Table 3.

Table 3) The model parameters used in case study II.			
Parameter	**Value (Unit)**	**Parameter**	**Value (Unit)**
k_1	0.001551	R_0	1 (Ω)
k_2	0.2818	R_1	20 (Ω)
k_3	−0.9754	R_M	4.5 (Ω)
k_4	0.001177	E	15 (V)
L	250 (mH)		

The result for the capacitor voltage is plotted versus time in Fig. 7. Similar to the previous case study, the multistage IDTM seems to have the best accuracy for a fixed step time.

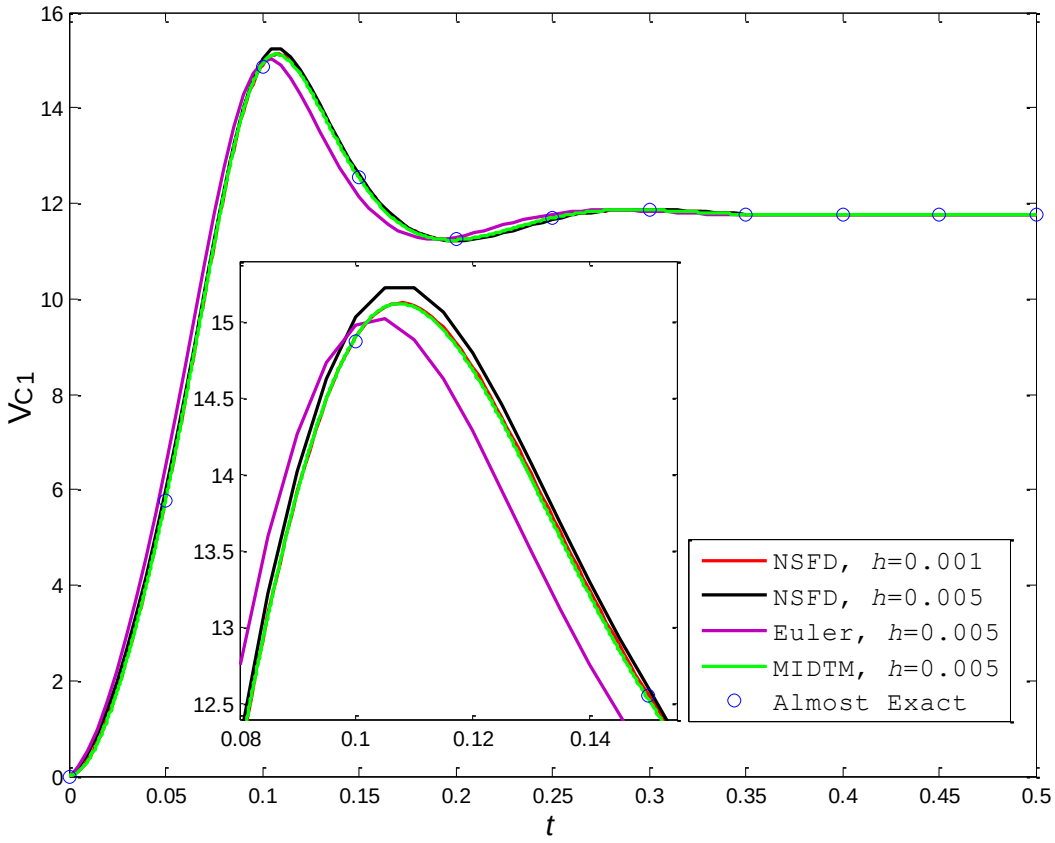

Figure 7) The solution of the inductive load case, i.e. Eq. (43), by the NSFD method, the Euler method, and the multistage improved differential transform method (MIDTM).

3.2.4. Error Analysis

Unlike Eq. (28), the system of nonlinear ODEs (43) cannot be solved analytically even in an implicit way. Therefore, we have to accept the numerical solution provided by the Euler method with a very small step size, i.e. 1e-10, as the almost exact solution. Next, we define the sum of absolute residual error as

$$E(N)=\sum_{n=0}^{N}\left|y_i-y_{\mathrm{AE},i}\right|, \tag{51}$$

where the subscript AE stands for the almost exact solution.
Consequently, the average of the absolute residual error is simply obtained by

$$\bar{E}(N)=\frac{1}{N+1}\sum_{n=0}^{N}\left|y_i-y_{\mathrm{AE},i}\right|. \tag{52}$$

Table 4 presents the error values of the three applied solution methods for case study II. Similar conclusions as in Section 3.1.4 can be drawn again. The multistage IDTM is desirably accurate, while the NSFD method is more reliable as its convergence is not affected by the step size selection. The performance of the Euler method is average from the computational viewpoint considering the CPU-times, the accuracy and the convergence behavior.

Table 4) Error analysis results of Eq. (15) for the time interval [0 0.5].

Method	***h***	$E(N)$	$\bar{E}(N)$	**CPU-time***
NSFD	0.001	0.0908	0.0091	0.002862
Euler		0.2813	0.0281	0.002878
MIDTM		0.0066	6.5883e-04	1.427164
NSFD	0.005	0.4541	0.0454	0.000457
Euler		1.4126	0.1413	0.000402
MIDTM		0.0606	0.0061	0.107681
NSFD	0.05	7.6595	0.7659	0.000065
Euler		Diverges	Diverges	Diverges
MIDTM		0.6208	0.0621	0.054464
NSFD	0.1	30.7057	3.0706	0.000036
Euler		Diverges	Diverges	-
MIDTM		Diverges	Diverges	-

* CPU-times are measured in seconds on a personal computer with a 2.66 GHz Intel® Core 2 Duo processor and 2.00 GB of RAM.

4. Conclusion

The voltage dynamics of an electrochemical battery was theoretically investigated by including a nonlinear capacitor in the classical Thévenin model as a modification. A new time-marching algorithm was developed based on the improved differential transform method to treat the proposed model. In addition to the conventional Euler method, the nonstandard finite difference schemes were devised to enable a comprehensive comparative study. Two separate case studies regarding a constant current consuming element and an inductive load on the system were addressed. It was revealed that the multistage IDTM posses the highest order of accuracy in spite of being computationally demanding. The latter, however, may not be considered a challenging issue in the presence of today's fast processors. On contrary, the NSFD method was found to be

very fast because its convergence is not affected by the increase of the discretization step sizes. Nevertheless, the NSFD could deliver acceptably accurate simulation results.

References

[1] M. Dürr, A. Cruden, S. Gair, J.R. McDonald, Dynamic model of a lead acid battery for use in a domestic fuel cell system, J. Power Sources 161 (2006) 1400-1411.
https://doi.org/10.1016/j.jpowsour.2005.12.075

[2] L. Lu, X. Han, J. Li, J. Hua, M. Ouyang, A review on the key issues for lithium-ion battery management in electric vehicles, J. of Power Sources 226 (2013) 272-288.
https://doi.org/10.1016/j.jpowsour.2012.10.060

[3] T. Hu, B. Zanchi, J. Zhao, Simple analytical method for determining parameters of discharging batteries, IEEE T. Energy Conver. 26 (2011) 787-798.
https://doi.org/10.1109/TEC.2011.2129594

[4] Z. M. Salameh, M. A. Casacca, W. A. Lynch, A mathematical model for lead-acid batteries, IEEE T. Energy Conver. 7 (1992) 93-98.
https://doi.org/10.1109/60.124547

[5] R. Xiong, H. He, K. Zhao, Research on an online identification algorithm for a Thevenin battery model by an experimental approach, Int. J. Green Energy 12 (2015) 272-278.
https://doi.org/10.1080/15435075.2014.891512

[6] H. Pang, L. Guo, L. Wu, X. Jin, An enhanced temperature-dependent model and state-of-charge estimation for a Li-Ion battery using extended Kalman filter, Int. J. Energ. Res. (2020) [in press]
https://doi.org/10.1002/er.5435

[7] Z. Wu, M. Shang, D. Shen, S. Qi, SOC estimation for batteries using MS-AUKF and neural network, J. Renew. Sustain. Ener. 11 (2019) 024103.
https://doi.org/10.1063/1.5064479

[8] G. Plett, Extended Kalman filtering for battery management systems of LiPb-based HEV battery packs part1: Background, J. of Power Sources 134 (2004) 252-261.
https://doi.org/10.1016/j.jpowsour.2004.02.031

[9] H. Chaoui, C. C. Ibe-Ekeocha, H. Gualous, Aging prediction and state of charge estimation of a LiFePO4 battery using input time-delayed neural networks, Electr. Pow. Syst. Res. 146 (2017) 189-197.
https://doi.org/10.1016/j.epsr.2017.01.032

[10] C. Burgos, D. Saez, M. E. Orchard, R. Cárdenas, Fuzzy modelling for the state-of-charge estimation of lead-acid batteries, J. of Power Sources 274 (2015) 355-366.
https://doi.org/10.1016/j.jpowsour.2014.10.036

[11] A. Salkind, C. Fennie, P. Singh, T. Atwater, D. Resiner, Determination of state-of-charge and state-of-health of batteries by fuzzy logic methodology, J. of Power Sources 80 (1999) 293-300.
https://doi.org/10.1016/S0378-7753(99)00079-8

[12] S.M. Mousavi G., M. Nikdel, Various battery models for various simulation studies and applications, Renew. Sust. Energ. Rev. 32 (2014) 477-485.
https://doi.org/10.1016/j.rser.2014.01.048

[13] S. Piller, M. Perrin, A. Jossen, Methods for state-of-charge determination and their applications, J. of Power Sources 96 (2001) 113-120.
https://doi.org/10.1016/S0378-7753(01)00560-2

[14] J. Zhou, Differential Transformation and its Applications for Electrical Circuits (in Chinese), Huazhong University Press, Wuhan, 1986.

[15] G. E. Pukhov, Differential Transformations and Mathematical Modeling of Physical Processes, Naukova Dumka, Kiev, 1986.

[16] H. Fatoorehchi, H. Abolghasemi, Improving the differential transform method: a novel technique to obtain the differential transforms of nonlinearities by the Adomian polynomials, Appl. Math. Model. 37 (2013) 6008-6017.
https://doi.org/10.1016/j.apm.2012.12.007

[17] G. Adomian, Solving Frontier Problems of Physics: The Decomposition Method, Kluwer Academic, Dordrecht, 1994.

[18] H. Fatoorehchi, H. Abolghasemi, An explicit analytic solution to the Thomas–Fermi equation by the improved differential transform method, Acta Phys. Pol. A 125 (2014) 1083-1087.
https://doi.org/10.12693/APhysPolA.125.1083

[19] H. Fatoorehchi, H. Abolghasemi, An integration-free method for inversion of Laplace transforms: A useful tool for process control analysis and design, Chem. Eng. Commun. 203 (2016) 822-830.
https://doi.org/10.1080/00986445.2015.1107722

[20] M. Areiza-Hurtadoa, D. Aristizábal-Ochoa, Large-deflection analysis of prismatic and tapered beam-columns using the Differential Transform Method, Structures 28 (2020) 923-932.
https://doi.org/10.1016/j.istruc.2020.09.034

[21] M. Ghafarian, A. Ariaei, Free vibration analysis of a system of elastically interconnected rotating tapered Timoshenko beams using differential transform method, Int. J. Mech. Sci. 107 (2016) 93-109.
https://doi.org/10.1016/j.ijmecsci.2015.12.027

[22] M. Kumar, G. J. Reddy, N. N. Kumar, O. A. Bég, Application of differential transform method to unsteady free convective heat transfer of a couple stress fluid over a stretching sheet, Heat Tran. Asian Res. 48 (2019) 582-600.
https://doi.org/10.1002/htj.21396

[23] R. E. Mickens, Applications of nonstandard finite difference schemes, World Scientific, Singapore, 2000.

[24] R. E. Mickens, Nonstandard finite difference schemes for differential equations, J. Differ. Equ. Appl. 8 (2002) 823-847.
https://doi.org/10.1080/1023619021000000807

[25] K. F. Gurski, A simple construction of nonstandard finite-difference schemes for small nonlinear systems applied to SIR models, Comput. Math. Appl. 66 (2013) 2165-2177.
https://doi.org/10.1016/j.camwa.2013.06.034

[26] E. Hernandez-Martinez, H. Puebla, F. Valdes-Parada, J. Alvarez-Ramirez, Nonstandard finite difference schemes based on Green's function formulations for reaction–diffusion–convection systems, Chem. Eng. Sci. 94 (2013) 245-255.
https://doi.org/10.1016/j.ces.2013.03.001

[27] D. T. Wood, H. V. Kojouharov, D. T. Dimitrov, Universal approaches to approximate biological systems with nonstandard finite difference methods, Math. Comput. Simulat. 133 (2017) 337-350.
https://doi.org/10.1016/j.matcom.2016.04.007

[28] M. Ehrhardt, R. E.Mickens, A nonstandard finite difference scheme for convection–diffusion equations having constant coefficients, Appl. Math. Comput. 219 (2013) 6591-6604. https://doi.org/10.1016/j.amc.2012.12.068

[29] C. G. Wei, T. L. Ren, J. Zhu, L. T. Liu, A ferroelectric capacitor mathematical model for spice simulation, Integr. Ferroelectr. 64 (2004) 101-111. https://doi.org/10.1080/10584580490893691